Experimental Study of an Artificial Thermal Plume in the Boundary Layer. Part III: Dynamic Structure within the Plume

J. NOILHAN* AND B. BÉNECH

Centre de Recherches Atmosphériques, Laboratoire d'Aérologie n° 354, Campistrous, 65300 Lannemezan, France

(Manuscript received 6 February 1985, in final form 24 June 1985)

ABSTRACT

An experimental study of the dynamics within artificial thermal plumes rising in the boundary layer is presented.

In this third part, measurements just above the heat source and aircraft investigations in the plume aloft are used to reveal the internal structure of the airflow within the buoyant column. Analysis of the pressure perturbation obtained both by direct measurements and as a residual in the mean vertical motion equation for a plume, shows that the vertical pressure gradient accelerates the airflow near the heat source and then reduces the buoyancy in the upper levels. The pressure deficits, attaining maximum values of 1 mb in the core of the lower portion of the plume, are well correlated with large vertical velocities. During light ambient wind conditions, the reduced pressure near the heat source produces a large converging inflow sufficient to cause the lower portion of the plume to go into rotation as a whole. An analysis of the components of the velocity field and momentum fluxes within the column underscores the convergent and divergent characters of the flow, respectively, at the lower and upper portions of the plume. Strong vorticity concentration ($\sim 4\ 10^{-2}\ s^{-1}$) is associated with a reduction of entrainment into the column.

1. Introduction

The airflow within a thermal plume strongly influences the transfer of thermodynamic quantities to the environment. That the dynamical processes which drive the ascending plume involve very complex mechanisms of airflow has already been shown by investigations of dust devils (Kaimal and Businger, 1970) and within a field of natural thermals (Lenschow and Stephens, 1980). These previous works have suggested that a major role is played by the perturbation of the pressure field and by the circulation in the dynamics of natural well-organized convective events.

Artificial convection represents an original way to study and understand the important thermodynamic processes leading to the dilution of a thermal perturbation in the boundary layer. However, few works have reported direct measurements of the dynamic characteristics of artificial plumes.

Some observational results within cooling tower plumes (Miller, 1977; Tun Ngem Chin, 1978) and large fires (Graig et al., 1979; Palmer, 1981) have shown that the heat source generates strong vorticity patterns which propagate upward into the convective column, resulting in reduced exchanges with the environment. During the operation Euroka fire (Williams et al., 1970), a vortex generated just above the fire was associated with a central pressure deficit of about 2 mb.

However, the previously mentioned observations were limited by a lack of quantitative and complementary measurements within the plume and the surrounding atmospheric layer, precluding a complete view of the dynamics of the plume as a function of the environmental conditions. In this paper, we present a picture of the overall dynamics of an artificial thermal plume rising in the boundary layer. The plumes were generated by a strong heat source of about 1000 MW at ground level. Analyses of the plume structure in the near vicinity of the heat source and within the convective column have already been presented by Bénech et al. (1986) and Noilhan et al. (1986) (hereafter referred to as I and II, respectively).

The present work adds another aspect to the previous experimental studies. Instrumentation at the base of the plume (25 and 50 m) has enabled us to observe the mean and turbulent characters of the airflow just above the heat source (I). Aircraft measurements within the convective column have been used to develop a statistical analysis of the vertical thermodynamical structure of the plume aloft (II). This third part attempts to tie together the measurements in the lowest 50 m and the aircraft observations of the plume aloft during conditions of light ambient wind. We discuss the importance of the pressure perturbation to the dynamics of the plume. This was estimated by direct airborne measurements and by a budget analysis. The study of the

* Present address: Centre National de Recherche de la Météorologie, Avenue Corriolis, 31057 Toulouse Cedex, France.

main patterns of the components of the airflow showing large convergence and vorticity within the lower portion of the column is then presented.

2. Techniques of analysis

Detailed measurements of the thermodynamic structure of the artificial thermals and the surrounding environment were obtained by means of aircraft penetrations of the rising column. The data analyzed here are for 10 experimental burns performed during June and July 1978. A description of the experimental techniques and the main characteristics of the boundary layer encountered during the experiments are to be found in I and II.

The plumes investigated could be clearly identified from the surrounding boundary layer by the perturbations of the temperature and vertical velocity (see II for details). The aircraft data provide good estimates of the pressure and velocity fields along a line through the thermal. The aircraft traverses, usually made along the wind, enable the description of the internal structure from its upwind to downwind parts. However, some transverse plume penetrations were made during light ambient wind conditions to investigate the cross-sectional structure of the column. The estimation of the longitudinal U' and transverse V' horizontal fluctuations of the flow is done after determining the mean horizontal wind vector $\mathbf{U}_a$ along each track (accuracy ± 1 m s^{-1}). The estimation of the fluctuations U' and V' of the instantaneous wind vector is done in the $\mathbf{U}_a$ reference frame (Létrenne, 1982).

A schematic representation of the processing of each parameter X are summarized in Fig. 1.

Each instantaneous parameter X is expressed as

$$X = \overline{X_a} + X_p, \tag{1}$$

where $\overline{X_a}$ is the mean value of X estimated outside the plume and X_p is the perturbed value within the plume. It is composed of a mean value $\overline{X_p}$ plus a fluctuating component X', where

$$\overline{X_p} = \frac{1}{l(z)} \int_{x_a}^{x_b} X_p dx, \tag{2}$$

with $l(z) = x_b - x_a$.

Here, $l(z)$ is the width of the active part of the plume and (x_a, x_b) the abscissae which delineate the thermal. The width $l(z)$ is defined as the horizontal length of the upwind zone wherein at least 80% of the heat flux occurred (II). The length $l(z)$ can be expressed as $\alpha D(z)$ where $D(z)$ is the distance from the source at height z. The length $D(z)$ takes into account the mean ambient flow $\overline{U_a}$ (see I for details). The entrainment coefficient α has been experimentally fixed at 0.23 (II).

The fluctuations X' are obtained by filtering the X_p time series with a high pass filter having a cut off of about 2 Hz.

The total covariance of the variables X_p and Y_p within the plume is defined as

$$\overline{X_p Y_p} = \frac{1}{l(z)} \int_{x_a}^{x_b} X_p Y_p dx, \tag{3}$$

and can be broken down into mean advective $\overline{X_p}\,\overline{Y_p}$ and turbulent $\overline{X'Y'}$ components.

The instantaneous longitudinal U_p, transverse V_p and vertical W_p components of the perturbed airflow within the column are determined in the external wind flow reference. An example of the variations of the U_p, V_p, W_p components along a transverse leg through the

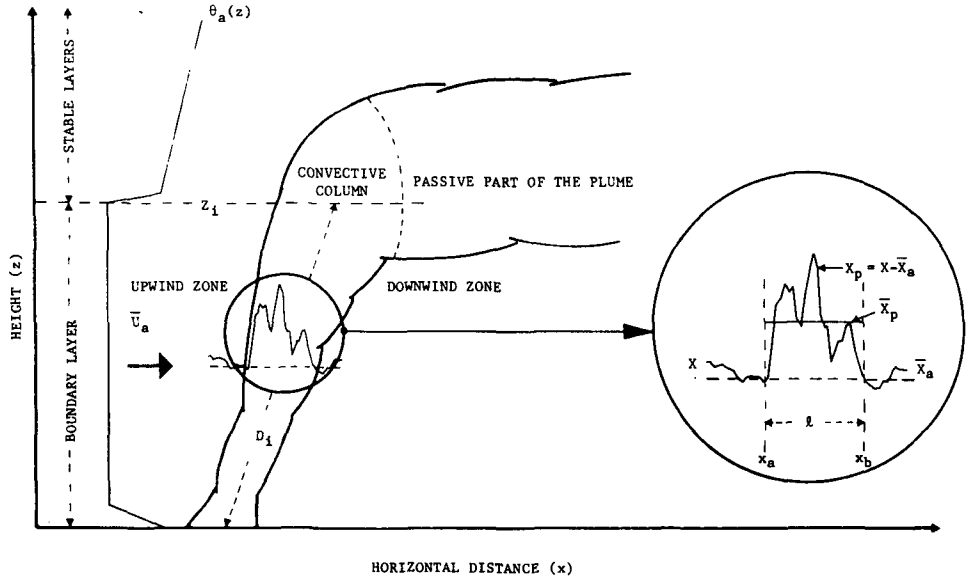

FIG. 1. Illustration of the different parts of the plume rising in the boundary layer and the capping stable layers. A schematic representation of the data processing within the convective column is given.

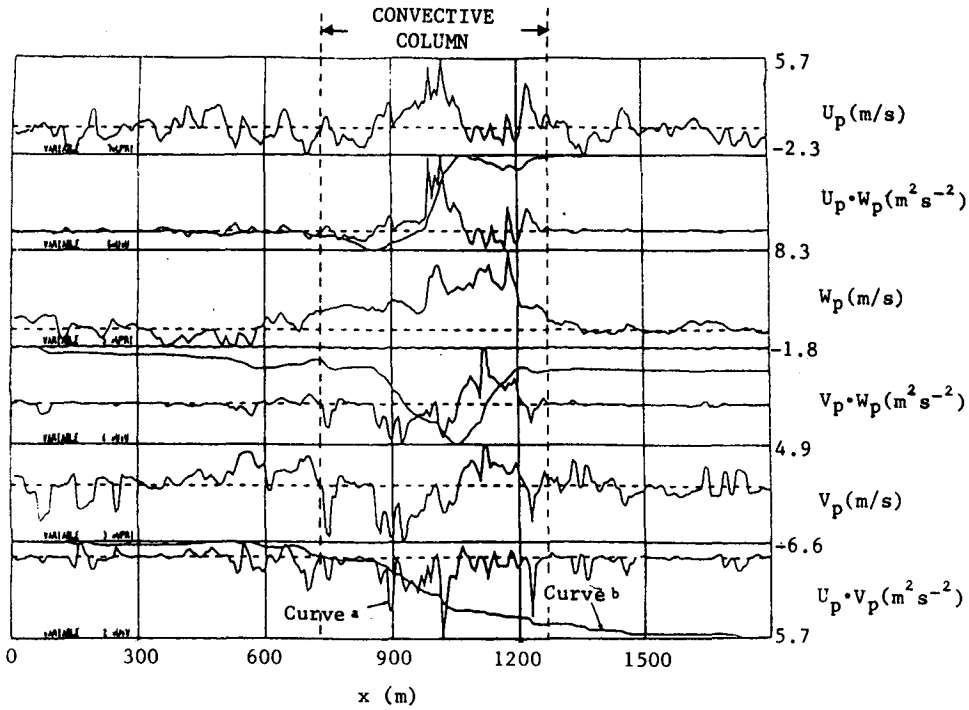

FIG. 2. Horizontal variations of the velocity components U_p, V_p, W_p and their corresponding total momentum fluxes along a flight leg through the plume. (For the covariance instantaneous product (curve a) and the horizontal integration $\int x_p y_p dx$ are plotted.) ($Z \approx 500$ m, 22 June 1978, aircraft speed $\sim$60 m s^{-1}.)

plume is given in Fig. 2. Instantaneous values of the total momentum covariances U_pV_p, U_pW_p, V_pW_p and their integrals are plotted.

The pressure perturbation was estimated from the comparison of the barometric and inertial trajectories of the aircraft inside the plume. The barometric trajectory is determined from the variations of the static pressure (accuracy $\sim$0.5 mb, sensitivity $\sim$0.1 mb, sampling increment $\sim$0.25 mb).

An equivalent height Z_p is then deduced by means of the hydrostatic equation. The measurements of the fluctuations of the vertical acceleration of the aircraft provide the estimation of an inertial height Z_{acc} by double integration. The drift in the estimation of Z_{acc} is eliminated by low frequency coupling with the height Z_p. The residual $DZ = Z_p - Z_{acc}$, which is zero outside the plume, defines the magnitude of the pressure perturbation generated by the thermal. The sign of DZ refers to a reduced pressure (positive) or an overpressure (negative). An example of the variations of DZ, of the vertical velocity W_p and of the potential temperature θ_p along a horizontal leg including the plume is given in Fig. 3.

3. Pressure perturbation within the plume

Few previous works have addressed the influence of the pressure term on the dynamics of thermals, principally due to the experimental difficulties. From the equation of the mean vertical velocity of a field of natural thermals, Kaimal and Businger (1970) and Lenschow and Stephens (1980) propose an estimation of the pressure gradient as a residual between acceleration and buoyancy terms. Their results suggest that pressure gradients must play an important role in driving the flow within the thermals. During the COCAGNE program, significant values of pressure perturbations were obtained in the more active zone of the plume under conditions of moderate ambient wind. In these cases,

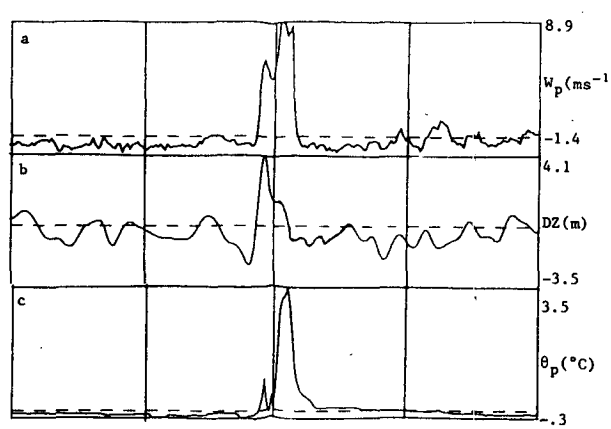

FIG. 3. Horizontal variations of DZ (a), W_p (b) and θ_p (c) within the column at 380 m.

we determined deficits to up to about 1 mb ($DZ \approx 10$ m). These peaks were generally associated with the maximum of the vertical velocity (see Fig. 3). This characteristic is shown in Fig. 4, which illustrates the high correlation between pressure perturbation and vertical velocity. Similar profiles were found in about half of the plume penetrations. The highest values of DZ measured at low levels ($Z \approx 300$ m) were associated with strong convergence and vorticity. It has been shown (I) that the horizontal and vertical accelerations of the airflow just above the source were strongly correlated, and this suggests the important role played by the pressure term in this region. The direct estimating of the pressure deficit at low levels seems to be in agreement with the previously mentioned observations.

From the lowest levels to the height where the pressure reduction effect is no longer detectable (500–600 m), the magnitude of the pressure perturbation monotonically decreases with a vertical gradient of about 0.1 mb/100 m.

The vertical profiles of $\overline{W_p}$, of the variance $\overline{W'^2}$ and of the buoyancy term can be used to examine the role of pressure in the equation for the mean vertical velocity. The vertical component of motion averaged over the plume, with the Boussinesq approximation, can be expressed as

$$\frac{\partial \overline{W_p}}{\partial t} + \frac{\overline{\partial W_p \cdot U_{pi}}}{\partial x_i} = -\frac{1}{\rho}\frac{\overline{\partial P_p}}{\partial z} + \chi\overline{\theta_p}, \qquad (4)$$

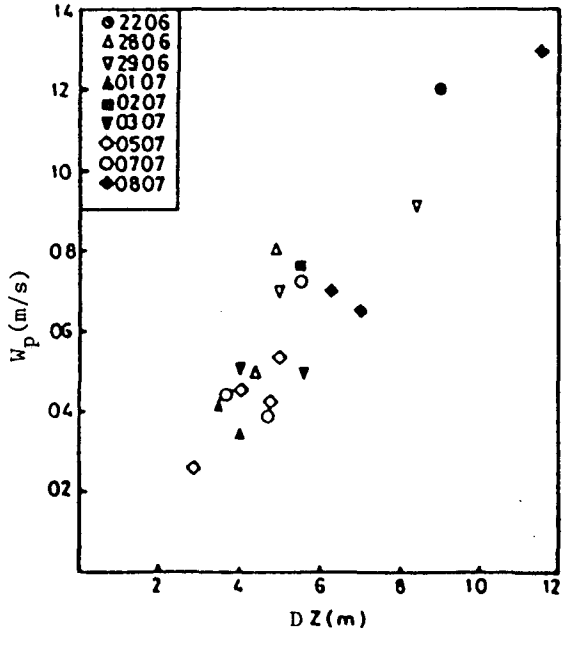

FIG. 4. A plot of W_p versus DZ showing the high degree of correlation between the equivalent height of the reduced pressure peak and the vertical velocity measured at the same instant within the plume (this graph corresponds to measurement heights less than 600 m).

where χ is the buoyancy parameter, ρ the air density, $\overline{\theta_p}$ the mean excess of the virtual potential temperature, and P_p the nonhydrostatic pressure within the plume.

In order to give an estimation of the pressure term in Eq. (4), we applied to our single plume an analysis similar to that developed by Lenschow and Stephens for a field of thermals. Equation (4) is derived in the vertical plane (x, z) where the x-axis is defined as the aircraft traverse axis (i.e., along the direction of the ambient wind). The transverse repartition (along y) of the properties of the plume is considered as symmetric about x axis, involving that the derivative of the terms with respect to y are zero. We assume steady state conditions and that the equation of continuity is satisfied within the plume, $\overline{\partial U_{pi}}/\partial x_i = 0$.

With the following properties for any perturbed variable X_p,

$$\overline{X'} = \frac{\partial \overline{X_p}}{\partial x} = 0.$$

The left-hand term of Eq. (4) can be expressed as

$$\frac{\overline{dW_p}}{dt} = \overline{W_p}\frac{\partial \overline{W_p}}{\partial z} + \overline{W_p}\frac{\partial \overline{W'}}{\partial z} + \frac{\overline{\partial W'^2}}{\partial z} + \frac{\overline{\partial W'U'}}{\partial x}. \qquad (5)$$

We expand Eq. (5) using the following averaging processes for the derivative with respect to x and z (the abscissa x_a, x_b of the plume edges are functions of z):

$$\frac{\partial \overline{X_p}}{\partial x} = \frac{1}{l(z)}(X_{pb} - X_{pa}), \qquad (6)$$

and

$$\frac{\overline{\partial X_p}}{\partial z} = \frac{\partial \overline{X_p}}{\partial z} + \frac{\overline{X_p}}{l(z)}\frac{\partial l(z)}{\partial z} - \frac{1}{l(z)}\left(X_{pb}\frac{\partial x_b}{\partial z} - X_{pa}\frac{\partial x_a}{\partial z}\right), \qquad (7)$$

where X_{pb} and X_{pa} are the instantaneous values of X_p at the edges x_b and x_a of the column.

Combining Eqs. (4), (5), (6), and (7), the equation of the vertical motion averaged over the plume can be written as

$$\overline{W_p}\frac{\partial \overline{W_p}}{\partial z} + \frac{\partial \overline{W'^2}}{\partial z} + \frac{\overline{W'^2}}{\rho(z)}\frac{\partial l(z)}{\partial z} + E_n = -\frac{1}{\rho}\frac{\overline{\partial P_p}}{\partial z} + \chi\overline{\theta_p}, \qquad (8)$$

with

$$E_n = \frac{1}{l(z)}\Big((U'W')_b - (U'W')_a + (W_pW')_a\frac{\partial x_a}{\partial z} - (W_pW')_b\frac{\partial x_b}{\partial z}\Big). \qquad (9)$$

The first and second left-hand terms of Eq. (8) represent the contribution for the acceleration from the turbulent fluctuations and the mean vertical velocity. The third term is a plume-size term which can be approximated during conditions of light ambient wind as $\overline{W'^2}/z$, considering that the width $l(z) = \alpha D(z) \approx \alpha Z$ (horizontal translation in such a case is negli-

gible, so that the distance $D(z)$ from the source to the height z is close to the z value).

The term E_n [expanded in Eq. (9)] represents the contributions of entrainment or detrainment through the plume edges and of the slopes of the edges. The effect of entrainment in E_n are taken into account by the horizontal gradient of the vertical momentum flux $U'W'$ between the edges of the plume. It will be shown in the next section that the horizontal flow in the lower portion of the plume is accelerated upwind and then decelerates downwind (convergence). This behavior appears to be reversed in the upper portion of the column (divergence). The convergence effect involves on the average that $U'_a > 0$ and $U'_b < 0$. If we consider that $W' < 0$ at the plume edges, we would expect that the first two terms of E_n are positive for entrainment and negative for detrainment. The last terms of E_n (contribution of the slope of the edges) are significantly smaller than the momentum terms since the slopes of the edges are about 0.1 for the plumes investigated.

It is not realistic, in this study, to obtain a precise estimate of E_n because the plume boundaries are not sufficiently well defined. Thus, the aircraft data permit one to compute entrainment fluxes only at a few data points. However, $|E_n|$ remains smaller than either of the other terms. Moreover, the lower portion of the plume analyzed was in rotation as a whole, causing reduced exchanges between the column and the surrounding layer.

In order to determine $-1/\rho(\overline{\partial P_p}/\partial z)$ as the residual of (8), we consider three experimental situations for which $\overline{U_a}$ was less than 3 m s^{-1} and the height Z_i of the boundary layer ranged between 700 and 1000 m (II). Normalized vertical profiles as a function of the reduced height D/D_i of the mean vertical velocity $\overline{W_p}$, root mean square σ_{W_p} and mean potential temperature excess $\overline{\theta_p}$ are given in Fig. 5.

The scaling parameters D_i (length scale; i.e., the distance from the source to z_i level), W_{p_*} (velocity scale) and θ_{p_*} (temperature scale) are the same as those presented in II. In case of light wind, D_i is close to height Z_i and w_{p_*}, θ_{p_*} are about 20 m s^{-1} and 30°C, respectively. One can also find in II a discussion of the ability of the scaling parameters to describe the thermodynamical structure of the plume in the boundary layer. In order to present a continuous profile from the heat source to the top of the boundary layer, continuity (dashed-line Fig. 5) is assumed between measurements made near the source (at about 0.025 and $0.05D/D_i$) and those made by the aircraft ($Z > 300$ m). In addition, infrared measurements (Brustet et al., 1980) were used to predict the range of the temperature excess at about $0.01D/D_i$ (Fig. 5c).

The vertical profile of $\overline{w_p}$ exhibits a rapid increase from the ground up to $0.2D/D_i$, followed by a slight decrease to D_i. The σw_p profile shows the same tendency but the maximum is obtained at a lower level (at about $0.1D/D_i$) and the decrease in the upper layer is more noticeable. The rapid decrease of $\overline{\theta_p}$ for $D < 0.4D_i$ is indicative of a high environment–thermal plume mixing in the lowest levels as it has also been shown in the profiles of the dissipative parameters (II). These profiles are now used to estimate the different terms of Eq. (8), normalized by D_i/W_*^2 (Fig. 6) through the whole boundary layer. The acceleration terms are of similar magnitude near the ground, but the deceleration of the divergence of the turbulent fluctuations is larger and appears at a lower level ($\sim 0.1D/D_i$) than that of the mean velocity divergence term. This behavior seems to be opposite to that found within natural thermals and indicates the strong dissipation in the lower layers induced by such an intense heat source. Figure 6 shows that the residual term near the ground level is positive, implying that $\overline{\partial P_p}/\partial z < 0$. Thus, the pressure term acts to accelerate the plume near the heat source. This is consistent with previous work on natural thermals. The pressure term is even larger than the buoyancy term and explains the strong acceleration found in the first 50 meters and the lack of significant pressure fluctuations at ground level (I).

Up to $0.05D_i$, $\overline{\partial P_p}/\partial z$ is positive. This is in agreement with the direct observations. In the upper part of the plume, the pressure term reduces the buoyancy of the thermal. Taking a mean value of $1/\rho(\overline{\partial P_p}/\partial z)$ equal to $0.02W_*^2/D_i$ at $0.5D/D_i$, we determine a mean gradient of about 0.1 mb/100 m. This represents a value about 100 times higher than the pressure gradients found within natural thermals (deduced from results presented by Lenschow and Stephens, 1980).

4. Concerning the airflow within the plume

This section considers some aspects of the mean and turbulent dynamics within the convective column. It describes what was observed under some favorable conditions, but not on every pass for various reasons, e.g., the aircraft did not always encounter exactly the center of the plume. In addition, the plume structure is not in a true steady state because of thermal pulsation of the heat source (I) and possible coupling between the column and the environment which infers a swaying of the whole column.

The present analysis is limited to situations where coupling was thought to be negligible (i.e., light wind, no horizontal entrainment by natural clouds). Figure 7 gives a general view of the main patterns of the dynamics within the column during light wind and without coupling (day 8 July 1978).

The airflow is illustrated from longitudinal legs (M1, M9) flown from about 300 to 950 m near the top of the plume (~ 1000 m). The time duration of the experimental flight was about 30 min. The magnitude of the vectors $\mathbf{V}(U_p, W_p)$ (Fig. 7a) and $\mathbf{V}(U_p, V_p)$ (Fig. 7b) has been calculated at horizontal intervals of approximately 8 m along each flight path. The legs M1 and M3, performed nearly at the same level, show a rela-

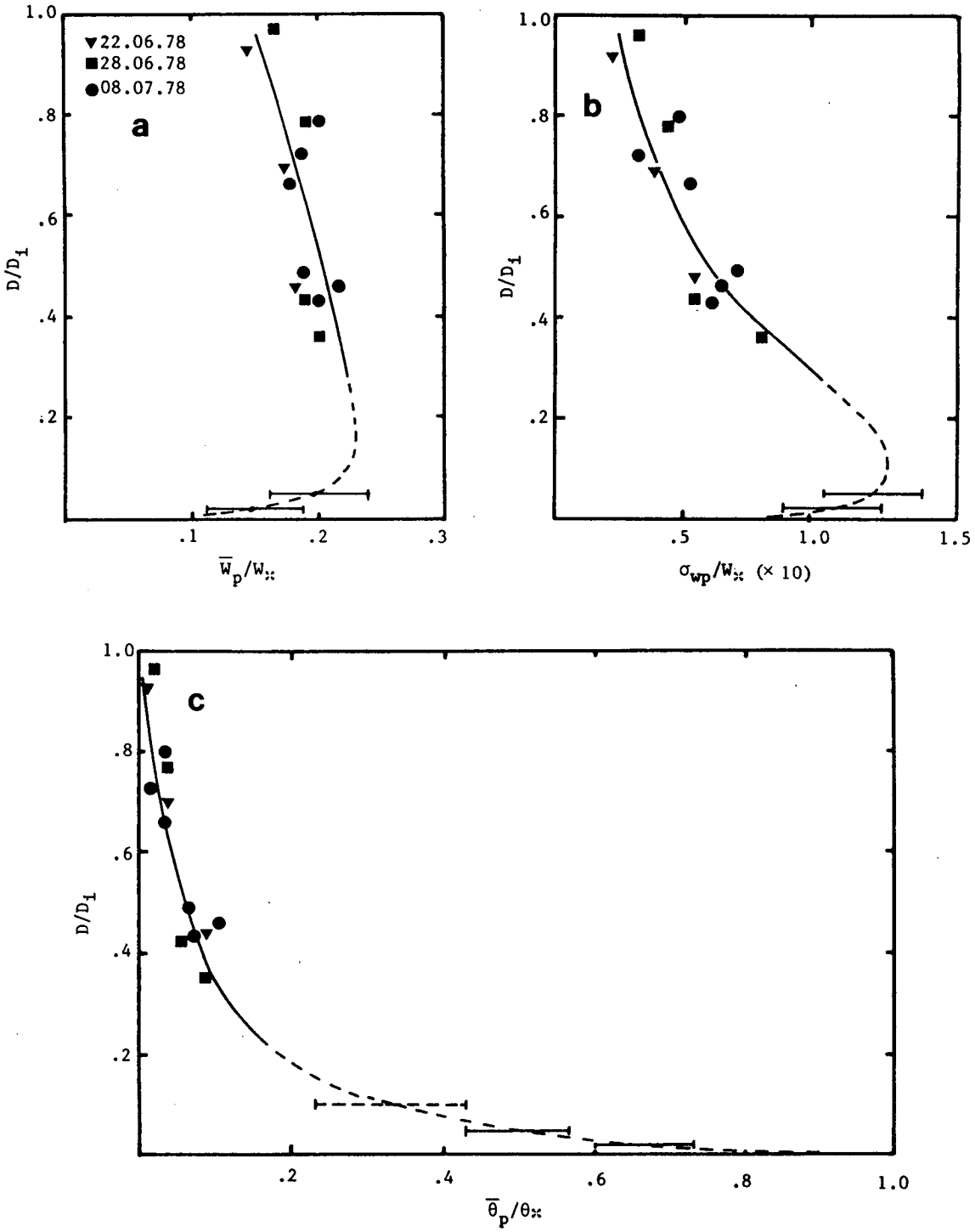

FIG. 5. Normalized vertical profiles of (a) $\overline{W_p}$, (b) σ_{wp} and (c) $\overline{\theta_p}$ versus the reduced height scale D/D_i. The short dashed lines (fitted by eye) suggest the continuity between the aircraft data ($D > 0.3D_i$) and measurements near the heat source.

tively high variability in the airflow due both to the internal plume structure and to the nonsimultaneous sampling. The airflow organization can be roughly divided into two zones. In the lower portion of the thermal plume (legs M9–M8), the vertical dynamical field [vector $\mathbf{V}(U_p, W_p)$] shows convergence of the airflow, highly localized at the plume edges. This convergence is associated with strong vorticity, as depicted by the

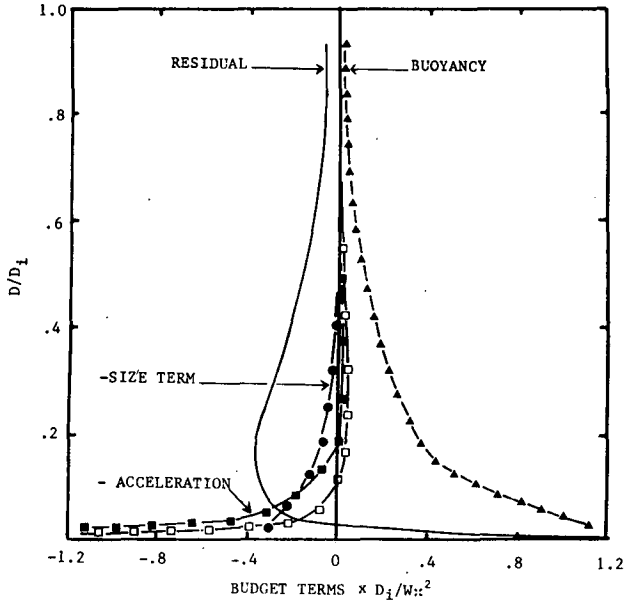

FIG. 6. Normalized terms in the vertical equation of $\overline{W_p}$ (8). Reversed profiles of the plume size term and acceleration terms are plotted.

horizontal dynamical field $\mathbf{V}(U_p, V_p)$ showing that the plume was in rotation as a whole. On the other hand, up to 500 m, the increase of the plume diameter is associated with a divergence of the vertical field [U_p is negative upwind and positive downwind—see for example $\mathbf{V}(U_p, W_p)$ variations in the leg M3] and a progressive disordering of the horizontal vorticity. In the present case, an artificial cloud was generated near the top of the convective column as was often observed in presence of a relatively dense field of natural cumulus (6/8 octa in this case). One could suspect that the low-level convergence may be enhanced by the formation of the small cumulus overhead.

a. *Convergence within the plume*

Figure 8 gives an example of the variations of U_p, W_p and U_pW_p at low (Fig. 8a) and high (Fig. 8b) levels. The legs presented correspond to along-the-wind aircraft passes at 500 and 950 m, respectively, through the same plume. For the both cases, the perturbed zone is delineated by $W_p > 0$.

The cross section at the lowest level (Fig. 8a) shows an upwind zone where W_p increases suddenly and U_p is positive, and a downwind zone where U_p becomes negative. In this last zone, the boundary of the plume is more diffuse as it is illustrated by the slow decrease of W_p downwind (case of a bent over plume, $\overline{U_a} \approx 5$ m s^{-1}). The associated vertical momentum flux U_pW_p is positive upwind and negative downwind since W_p is positive along the whole cross section of the column. On the other hand, in the upper level (Fig. 8b), the U_p and U_pW_p components are first negative then positive, in the upwind and downwind parts of the track, respectively. However, among the cases analyzed, the structure in the upper levels is not as clearly defined as at the lower ones. This is because during its rise the boundaries of the plume are being eroded away by mixing with the surrounding, resulting in a reduction of the magnitude of the various dynamic parameters. In Fig. 8b, the plume is still identifiable from its surroundings but the dynamic parameters are weak (maximum value of $W_p \sim 1.2$ m s^{-1}).

In the convergent region of the plume, the advected momentum flux $\overline{U_pW_p}$ is upward in the upwind part and downward in the downwind part of the column. In the upwind zone, maximum values of U_pW_p are obtained near the edge of the plume, leading to a mean positive value of $\overline{U_pW_p}$ of about 4 m^2 s^{-2}. These results can be compared with the observations of Kaimal and Businger (1970) who noted upward momentum transport mainly confined to the edges of the base of a dust devil. However, the reduction of W_p and U_p within the core of the dust devil reported by these authors or in numerical simulations (Smith and Leslie, 1976) is not clearly apparent in the analysis presented here. The convergence field near the base of the plume was well identified from the instrumented area just above the heat source (I). Radar and photogrammetry data (Sauvageot et al., 1980) have shown that this effect was maintained up to 300–400 m. A resulting contraction of the plume diameter and acceleration of the vertical velocity was verified experimentally (I) and previously observed by Benech (1976); these are well represented by simple numerical predictions of plume rise (Meltz et al., 1983). On the other hand, the divergent flow near the plume top involves an increase of the plume radius associated with a rapid decrease with height of the magnitude of the perturbed parameters (II).

b. *Vorticity within the plume*

Of the many airborne measurements analyzed, strong vorticity was found in only a few plumes and was associated with conditions in which the lower portion of the plume was in rotation as a whole. We have observed two particularly favorable situations (days 22 June and 8 July 1978) corresponding to light winds (~1–2 m s^{-1}) and thermal instability in the surface boundary layer. Vorticity in the lower portion of the plume for the day 8 June 1978 has been already depicted in Fig. 7b (legs M8–M9). In order to describe the internal dynamics of this type of circulation, we again turn to the data presented in Fig. 2. The two lateral sides of the plume exhibit values of U_p and V_p reversed in sign, e.g., in the left-half side $U_p > 0$ and $V_p < 0$, and in the right-half side $U_p < 0$ and $V_p > 0$. Among the cases analyzed, the distribution of V_p always has a characteristic pattern but gives the sense of rotation. For example, V_p is positive in the upwind zone

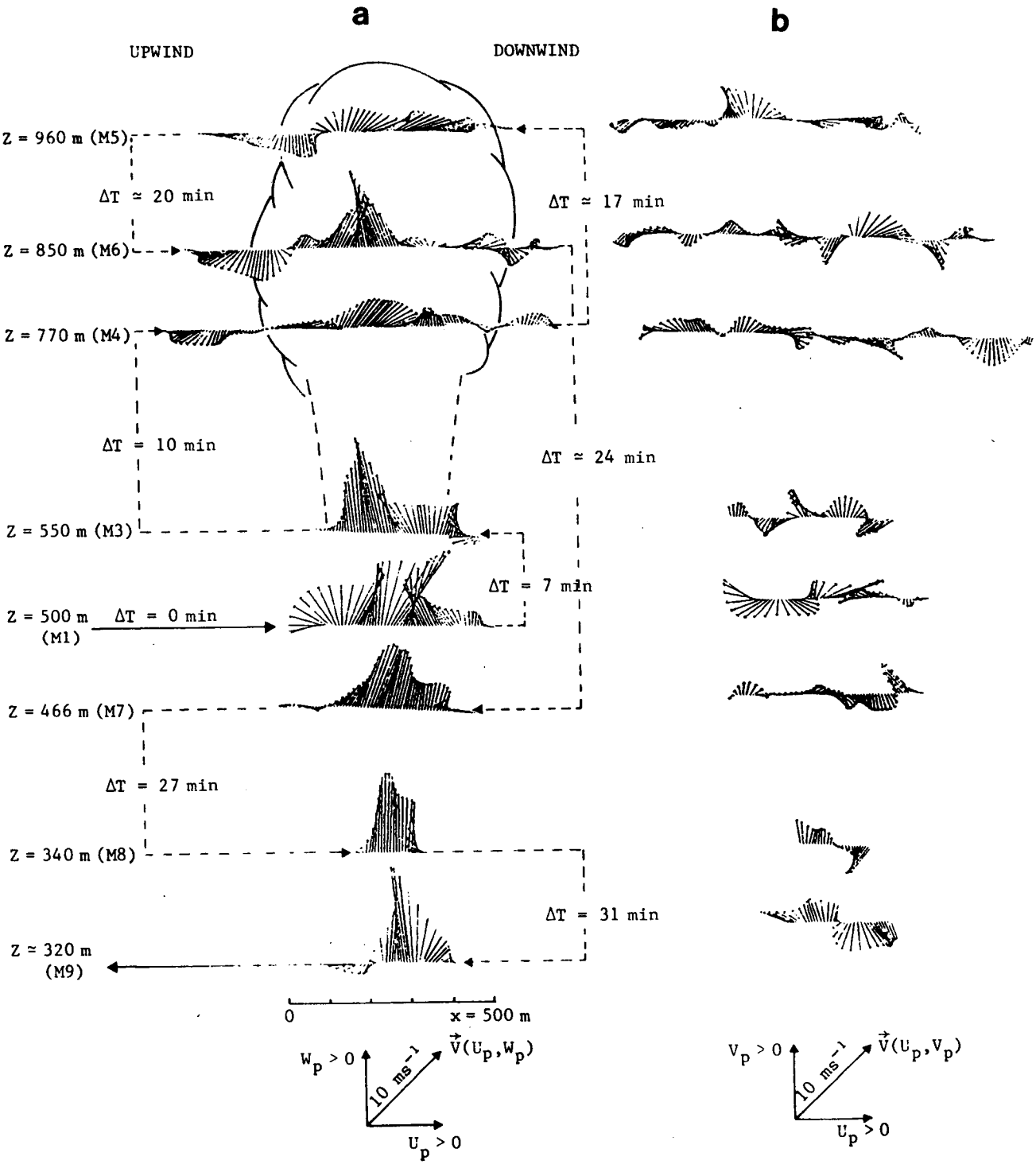

FIG. 7. Illustration of the airflow within a quasi-vertical convective column interacting with a natural cloudy cell. The horizontal variations of the vectors (a) $\mathbf{V}(U_p, W_p)$ and (b) $\mathbf{V}(U_p, V_p)$ along the paths (M1 . . . M9) through the plume are given. For each plume traverse the increment of time Δt(min) from the beginning of the aircraft investigations is indicated in (a).

for cyclonic rotation. The change in sign of both U_p and V_p between the two parts of the plume means that the sign of the product U_pV_p remains constant, resulting in a steady variation of the value of its integral along the path (for example, steady decrease of the integral of U_pV_p in Fig. 2).

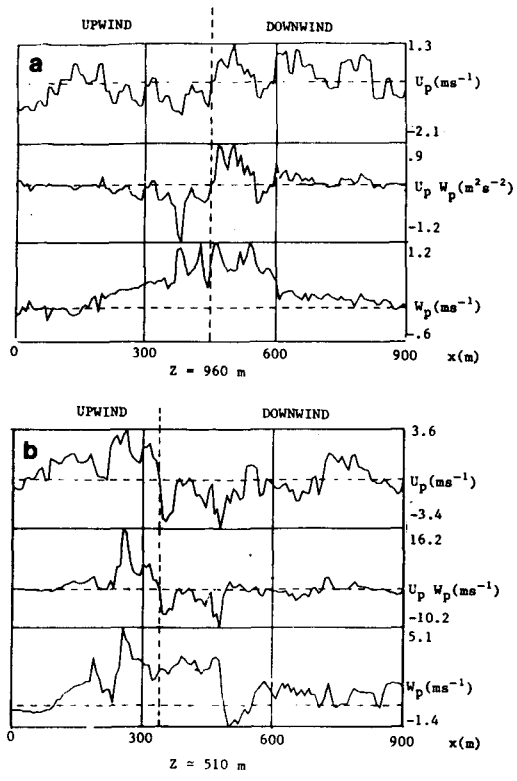

FIG. 8. Horizontal variations of the longitudinal U_p, vertical W_p and vertical momentum flux U_pW_p components along two legs flown at (a) low and (b) high levels for the same plume.

The well-organized vortex structures for the two experiments could be most clearly identified at low levels (<600 m). They were associated with strong convergence (Fig. 7a) and with relatively large pressure perturbation (~1 mb, see Table 1) within the core of the thermal plume. Church et al. (1980) have suggested that such a concentration of vertical vorticity is the result of strong low-level convergence. This serves to concentrate the weak background vertical vorticity. The analysis of pressure perturbation carried out in this paper underscores the production of a large converging inflow in the lower portion of the plume. It has been shown that pressure deficit was correlated with the magnitude of the vertical velocity W_p. Since during light wind conditions, the plume core is associated with large thermodynamic values (I), it is expected that the corresponding pressure reduction will involve large radial inflow sufficient to cause the rotation of the entire plume. In such a mechanism, the concentration of preexisting weak background vertical vorticity does not appear as a predominant factor.

The effect of the single line vortex was to limit the diameter of the plume to no more than 150 m (Table 1) for the two cases analyzed, since the rapid swirling of the air results in reduction of entrainment at low levels into the plume. Thus, the mass flux ascending in the buoyant plume is furnished principally by a shallow surface layer with intense radial inflow.

Table 1 summarizes the main dynamic characteristics of the paths analyzed when the column was in rotation as a whole. The order of magnitude of the vertical component ω of vorticity has been estimated from

$$\omega = 2\overline{V_T}/R, \tag{10}$$

where $\overline{V_T}$ is the tangential velocity and R the mean plume radius.

The values of ω thus derived are about 4 10^{-2} s^{-1}. They are comparable with the estimates from the horizontal airflow field nearer the heat source (I) and are on the same order of magnitude as estimates within natural thermals (Gaynor et al., 1963) and dust devils (Fitzjarrald, 1973) in the convective boundary layer. The mean tangential velocity of the vortices at the edge of the plume is about 2 m s^{-1}, approximately one half of the mean vertical velocity $\overline{W_p}$ during the day 8 June 1978. These estimates of $\overline{V_T}$ are comparable with those of Hanna et al. (1978), who made a photogrammetric study of a natural draft cooling tower.

5. Conclusion

Aircraft observations within artificial plumes have been used to evaluate several important features of the dynamics of thermals. Direct measurements of the pressure perturbations show reduced pressures in the core of the convective column, attaining maximum values of 1 mb in the lower portion of the plume. These reduced pressures are well correlated with large vertical velocities. Calculation of the terms in the mean momentum equation for a plume (acceleration, buoyancy and size terms) under light ambient wind conditions suggests the importance of the pressure gradient term. This acts to accelerate the plume near the heat source and to reduce the buoyancy in the upper levels. The derived vertical pressure gradient value of 0.1 mb/100

TABLE 1. Dynamic characteristics of the circulation within the convective column when it was in rotation as a whole.

Day	Height (m)	$\bar{V}_T$ (m s^{-1})	$\bar{W}_p$ (m s^{-1})	$\bar{R}$ (m)	ω (10^{-2} s^{-1})	P_p (mb)	$W_{p\max}$ (m s^{-1})
22 June 1978	510	3.1 ± 0.7	3.5	140	4.4 ± 0.8	−0.8	8.3
8 July 1978	320	2.3 ± 0.2	5.0	130	3.6 ± 0.4	−1.1	13
	340	1.8 ± 0.2	4.1	90	4 ± 0.5	−0.7	8.9

m within the column is in agreement with direct estimates. During light wind conditions, large pressure deficits lead to strong converging inflow in the lower portion of the plume. It is expected that these mechanisms cause the column to go into rotation as a whole. Strong vorticity concentration ($\sim 4 \times 10^{-2}$ s^{-1}) within the plume is associated with reduction of entrainment into the column.

Acknowledgments. This work was supported by a grant from Electricité de France, Division Etudes et Recherches.

We are grateful to Mr. Létrenne and Mr. Durand for their assistance with the data processing, to Mrs. Campistron and Mrs. Réchal for typing the manuscript. The authors are grateful to A. Druilhet, J. T. Snow and C. R. Church for stimulating discussions and for helpful review of the manuscript.

REFERENCES

Bénech, B., 1976: Experimental study of an artificial convective plume initiated from the ground. *J. Appl. Meteor.*, **15,** 127–137.

——, J. Noilhan, A. Druilhet, J. M. Brustet and C. Charpentier, 1985: Experimental study of an artificial thermal plume in the boundary layer. Part I: Flow characteristics near the heat source. *J. Climate Appl. Meteor.*, **25,** 418–437.

Brustet, J. M., and B. Bénech, 1980: Dépouillement des thermogrammes infrarouge collectés pendant COCAGNE 3. *Document de travail I.O.P.G.* 80.19, 30 pp.

Church, C. R., J. T. Snow and J. Dessens, 1980: Intense atmospheric vortices associated with a 1000 MW fire. *Bull. Amer. Meteor. Soc.*, **61,** 682–694.

Fitzjarrald, D. E., 1973: A field investigation of dust devils. *J. Appl. Meteor.*, **12,** 808–813.

Gaynord, J. E., F. F. Hall, J. R. Edinger and G. R. Ochs, 1977: Measurement of vorticity in the surface layer using an acoustic echo sounder array. *Remote Sens. Environ.*, **6,** 127–137.

Graig, C. D., and M. A. Wolf, 1979: An observational study of field burning plume behavior. *Air Resources Center,* Corvallis.

Hanna, S. R., M. Pike and K. Seitter, 1978: Observations of vortices in cooling tower plumes. *J. Appl. Meteor.*, **17,** 1068–1071.

Kaimal, J. C., and J. A. Businger, 1970: Case studies of a convective plume and dust devil. *J. Appl. Meteor.*, **9,** 612–620.

Lenschow, D. H., and P. L. Stephens, 1980: The role of thermals in the convective boundary layer. *Bound. Layer Meteor.*, **19,** 509–532.

Létrenne, G., 1983: Contribution à l'étude des structures moyennes et turbulentes d'un thermique artificiel dans la couche limite planétaire. *Thèse de 3ème cycle,* n° 2767, Toulouse.

Meltz, C., B. Bénech, J. P. Lacaux and P. Sarthou, 1983: Modèle unidimensionnel de nuage chaud. *Rapport Interne de l'I.O.P.G.* n° 67, 73 pp.

Miller, R. L., 1977: Characteristics of temperature fluctuations in cooling tower plumes. Ph.D. dissertation, University of Pennsylvania, 71 pp.

Noilhan, J., B. Bénech, G. Létrenne, A. Druilhet and A. Saab, 1985: Experimental study of an artificial thermal plume in the boundary layer. Part II: Some aspects of the plume thermodynamical structure. *J. Climate Appl. Meteor.*, **25,** 439–457.

Palmer, T. Y., 1981: Large fire winds, gases and smoke. *Atmos. Environ.*, **15,** 2079–2090.

Sauvageot, H., G. Lafon and M. Oruba, 1980: Thermal plume study using radar and chaff. *19th Conf. on Radar Meteorology,* Amer. Meteor. Soc., 662–669.

Smith, R. K., and L. M. Leslie, 1976: Thermally driven vortices: A numerical study with application to dust devil dynamics. *Quart. J. Roy. Meteor. Soc.*, **102,** 791–804.

Tun Ngem Chin, 1978: Characteristics of vertical velocities and vertical sensible heat fluxes in cooling tower plumes. Ph.D. thesis, Pennsylvania State University, 80 pp.

Williams, D. W., J. S. Adams, J. J. Batten, G. F. Whitty and G. T. Richardson, 1970: Operation Euroka, an Australian Mass Fire Experiment, Rep. 386, Defence Standards Lab., Maribyrnon, Victoria, Australia.